EFFECT OF DIFFERENT UPSTREAM FITTINGS ON ORIFICE METER PERFORMANCE

تأثير الوصلات المختلفة في أعلى السريان على أداء مقياس التصرف الفُوَّهى

A. A. Zahran[1], L. H. Rabie[2], I. M. Shabaka[3], and M. A. El-Naggar[4]

[1] Research Assistant, National Institute for Standards, Egypt

[2] Professor, Mechanical Power Engineering Department, Faculty of Engineering, Mansoura University, El-Mansoura, Egypt

[3] Professor, Aeronautical and Aerospace Engineering Department, Faculty of Engineering, Cairo University, Cairo, Egypt

[4] Assistant Professor, Mechanical Power Engineering Department, Faculty of Engineering, Mansoura University, El-Mansoura, Egypt

E-mails: eng_alizahran@yahoo.com; lotfyrs@hotmail.com; ishabaka@hotmail.com; naggarm@mans.edu.eg

الملخص:

إن مقياس التصرف الفُوَّهى هو أحد أنواع أجهزة قياس السريان المعتمِدة على قياس فرق الضغط ، والتي تستخدم على نطاق واسع في التطبيقات الصناعية المرتبطة بقياس حجم ومعدل السريان للسوائل عالية التكلفة مثل : الغاز الطبيعي ، البترول ، المياه. وتعتمد دقة قياس هذه الأجهزة بشكل أساسي على موضعها في شبكة الأنابيب. يهتم هذا البحث بدراسة تأثير ظروف السريان الغير قياسية المولّدة بمختلف الوصلات قبل الفوهة مثل : (مختزل السريان ، الكوع المفرد ، كوعان في نفس المستوى ، كوعان في مستويين متعامدين ، وصلة T) والتي تركب على مسافات مختلفة غير قياسية قبل العداد على منحنى السرعة ومعامل التصرف. لقد استخدمت كلاً من طرق الدراسة الرقمية والعملية للتحقق من هذه المسألة. وتشير النتائج إلى أن كل وصلة لها تأثير مختلف على منحنى السرعة ومعامل التصرف ، وأذكر كمثال : الكوع العمودي يقلل من معامل التصرف كلما قلت المسافة بينه وبين فتحة التصرف وكلما زاد رقم رينولدز ،

Accepted March, 5, 2013

وكذلك لا يتوافق منحنى السرعة كلياً مع المنحنى الطبيعي حتى بعد مسافة مستقيمة تساوي ٤٠ ضعف قطر الماسورة بين الكوع وفوهة التصرف.

محركات البحث:

فوهة التصرف ، معامل التصرف ، ظروف السريان الغير قياسية ، منحنى السرعة

Abstract

Orifice meters are a type of the differential pressure flow meter widely used in industrial applications dealing with measuring the size and flow rate of expensive fluids such as natural gas, petroleum and water. The measurement accuracy of these meters depends mainly on their position in a pipe network. This paper is concerned with the effect of nonstandard flow conditions generated by various fittings (e.g.: reducer, single elbow, double-elbow in-plane, double-elbow out-of-plane, T-junction) at different nonstandard upstream distances of the orifice plate on velocity profile and on discharge coefficient. Both numerical and experimental studies were used to investigate this problem. The results show that for each fitting, there is a different effect on the velocity profile and on the discharge coefficient. As an example, the 90^{o} elbows decreases the discharge coefficient with decreasing upstream distance and increasing Reynolds number. Also, after a straight distance of 40D between the elbow and the orifice plate, the velocity profile is not fully matched with the normal profile.

Keywords: Orifice meter, Discharge coefficient, Nonstandard flow conditions, Velocity profile

1. Introduction

Orifice meters are the most commonly used method in flow measurement, especially in industrial applications. It is also the most common of the differential pressure (DP) flow meter family. Differential-producer flow meters create a restriction in the flow field. When flow is contracted, either gradually or abruptly, kinetic energy increases at the expense of potential energy (static pressure).

It was noticed that the orifice meter readings (measurements) are affected by upstream fittings (single elbows, double elbows in-plane, double elbows out-of-plane, valves, reducers, expanders, T-pieces) especially if such fittings were located at an upstream distance less than

that which assures a fully-developed flow, i.e. a steady flow free of swirl and where the velocity profile does not change along axial direction. Fittings lead to disturbances.

ISO 5167(2003) standard provides tables for the decay lengths depending on the pipe fittings. However, there is no information in the standard on the relationship between the decay length and the Reynolds number. Orifice meters are simply designed [see Fig. (1).] and built on the basic relation between the pressure difference across the orifice plate and the flow rate (flow velocity). This theoretical relationship is corrected using the discharge coefficient C_d. It is of major interest for manufacturers of flow meters as well as for meter users to know before the actual installation how the meter reacts to a specific flow disturbance.

Numerous works have been performed and reported in the literature. Prabu et al. (1996) carried out their experiments to investigate the effect of upstream pipe fittings such as a single 90^{o} bend, double 90^{o} bends in plane and double 90^{o} bends out-of-plane on the performance of a conical flowmeter and orifice meter. The most significant conclusions drawn from their study are that an upstream piping of at least 11 pipe diameters length is necessary to separate the orifice meter, from a single 90^{o} bend and a double 90^{o} bend (in-plane), and upstream piping of at least 48 pipe diameters is required for a double-bend out-of-plane disturbance for both the conical flowmeter and orifice meter.

Mattingly and Yeh (1991) presented experimental results for the decay of pipe elbow produced swirl in pipe flows and its effects on flowmeter measurement accuracy. Experiments include the decay of swirl produced by single and double-elbow configurations for pipe diameter Reynolds numbers of 10^4 to 10^5 using water in a 50 mm diameter facility at National Institute of Standards and Technology (NIST) in USA. Results show that different types of swirl are produced by the different piping configurations. The swirl decay is found to be dependent on the type of swirl and the pipe Reynolds number. Without flow conditioning, it is concluded that the specifications of upstream pipe lengths in the current flow metering standards may not be sufficient to achieve the desired flow metering accuracy.

Reader-Harris et al. (1995) carried out work to derive an improved orifice plate discharge coefficient equation based on the enlarged European Economic Community / American Petroleum Institute (EEC/API) database including the data collected in 50

and 600 mm pipes. It consists of several terms, each based on an understanding of the physics. An earlier version of this equation, based on a smaller database, was accepted at a meeting of EEC and API flow measurement experts in New Orleans in 1988, and emphasis is placed on the two principal changes to the equation: improved tapping terms for low Reynolds number have been calculated; and an additional term for small orifice diameter has been obtained.

Also, Reader-Harris/Gallagher (1998), as presented in ISO 5167(2003), gave an equation for the discharge coefficient, C_d.

Rhinehart et al. (2011) considered the complexity of the 28-coefficients Reader-Harris/Gallagher equation and the 8–coefficient expansibility relation all add potential for implementation error. Engineering practice desires to minimize potential for error. Since the discharge coefficient depends on Reynolds number, the use of the ISO procedure is iterative (flow rate is required to calculate C_d, but C_d is required to calculate flow rate), which adds implementation complexity and requires a convergence criterion. Engineering practice desires to minimize complexity. Finally, standard relations require the orifice pressure drop as the input to the calibration equation. They introduced the power law relation to replace the square root relation in the orifice flow rate calculation for noncompliant devices.

Gersten (2008) introduced the characteristic parameters which allow an appropriate description of the flow disturbances in order to solve the problem of flow metering that disturbed by pipe fittings (e.g. bends) and the decay length is not available. These characteristic parameters can be determined experimentally by measuring the circumferential distributions of the wall shear stress components. This can be done by sublayer fences, Preston tubes or surface hot films.

Yoon et al. (2009) investigated the effect of distance between 90° elbow close to the upstream face of an orifice plate and the orifice plate on discharge coefficient experimentally by comparing the master flow meter and another testing machine. Using the master flow meters with flow rate of range 0.3 – 25 m^3/h, they gave results for the case of short distance between the elbow and the orifice plate, the deviation of the discharge coefficient tended to increase over 5%. As the distance between the elbow and orifice plate was increased, the discharge coefficient was closer to the reference value and the deviation was reduced

especially, in the case of the flow with Reynolds number $6x10^4$. If the distance between the elbow and the orifice plate was 18D at Reynolds number less than $6x10^4$ the deviation of the discharge coefficient was close to 1% of the reference value. With a Reynolds number over $6x10^4$, a straight pipe length is needed of over 18D to recover the discharge coefficient.

National Institute of Standards and Technology (NIST) in USA made a data base (1994) for flanged orifice types for various fluids that included water, gas, oil, and natural gas. These data were collected by NIST for the purpose of generating international standard producers to calibrate orifice meters, and to provide researchers and the industries with an archive of traceable data.

The aim of this study is to examine experimentally and numerically the effect of fittings on the flow structure of upstream and downstream of the orifice plate. It is objected also to investigate the influence of elbow and other fittings on the discharge coefficient of the orifice meter.

2. Numerical Study

The numerical investigation for a steady - state flow of a Newtonian fluid with constant density and viscosity is based on the two main equations, namely: the continuity equation, and Navier-Stokes equations in the following forms:

Continuity equation:

The differential form of the continuity equation in cylindrical coordinates for incompressible fluids is:

$$\frac{1}{r}\frac{\partial(r\upsilon_r)}{\partial r}+\frac{1}{r}\frac{\partial \upsilon_\theta}{\partial \theta}+\frac{\partial \upsilon_z}{\partial z}=0 \qquad (1)$$

Navier-Stokes equations:

Navier-Stokes equations are considered to be the governing differential equations of motion for incompressible Newtonian fluids. In terms of cylindrical coordinates, the Navier-Stokes equations for steady state can be written as in Eq. (2).

$$(r-direction)$$

$$\rho\left(\upsilon_r\frac{\partial \upsilon_r}{\partial r}+\frac{\upsilon_\theta}{r}\frac{\partial \upsilon_r}{\partial \theta}-\frac{\upsilon_\theta^2}{r}+\upsilon_z\frac{\partial \upsilon_r}{\partial z}\right)$$
$$=-\frac{\partial p}{\partial r}+\rho g_r+\mu\left[\frac{1}{r}\frac{\partial}{\partial r}\left(r\frac{\partial \upsilon_r}{\partial r}\right)\right.$$
$$\left.-\frac{\upsilon_r}{r^2}+\frac{1}{r^2}\frac{\partial^2 \upsilon_r}{\partial \theta^2}-\frac{2}{r^2}\frac{\partial \upsilon_\theta}{\partial \theta}+\frac{\partial^2 \upsilon_r}{\partial z^2}\right]$$

$$(\theta-direction)$$

$$\rho\left(\upsilon_r\frac{\partial \upsilon_\theta}{\partial r}+\frac{\upsilon_\theta}{r}\frac{\partial \upsilon_\theta}{\partial \theta}+\frac{\upsilon_r\upsilon_\theta}{r}+\upsilon_z\frac{\partial \upsilon_\theta}{\partial z}\right)$$
$$=-\frac{1}{r}\frac{\partial p}{\partial \theta}+\rho g_\theta+\mu\left[\frac{1}{r}\frac{\partial}{\partial r}\left(r\frac{\partial \upsilon_\theta}{\partial r}\right)\right.$$
$$\left.-\frac{\upsilon_\theta}{r^2}+\frac{1}{r^2}\frac{\partial^2 \upsilon_\theta}{\partial \theta^2}+\frac{2}{r^2}\frac{\partial \upsilon_r}{\partial \theta}+\frac{\partial^2 \upsilon_\theta}{\partial z^2}\right]$$

$(z-direction)$

$$\rho\left(v_r\frac{\partial v_z}{\partial r}+\frac{v_\theta}{r}\frac{\partial v_z}{\partial \theta}+v_z\frac{\partial v_z}{\partial z}\right)$$
$$=-\frac{\partial p}{\partial z}+\rho g_z+\mu\left[\frac{1}{r}\frac{\partial}{\partial r}\left(r\frac{\partial v_z}{\partial r}\right)\right.$$
$$\left.+\frac{1}{r^2}\frac{\partial^2 v_z}{\partial \theta^2}+\frac{\partial^2 v_z}{\partial z^2}\right] \quad (2)$$

Navier-Stokes equations and continuity equation were solved using Fluent three-dimensional double precision (3ddp) with full simulation mode Computational Fluid Dynamics (CFD) code version 6.3.26 to get the computational solution for the problem under investigation.

The Realizable k-ε Turbulence Model were implemented to solve this problem. This model more accurately predicts the spreading rate of both planar and round jets. It is also likely to provide superior performance for flows involving rotation, boundary layers under strong adverse pressure gradients, separation, and recirculation. The modeled transport equations for k-ε turbulence model are presented in Eqs. (3) and (4).

$$\frac{\partial}{\partial x_j}\left(\rho k u_j\right)=\frac{\partial}{\partial x_j}\left[\left(\mu+\frac{\mu_t}{\sigma_k}\right)\frac{\partial k}{\partial x_j}\right]$$
$$+\mu_t S^2-\rho\varepsilon \quad (3)$$

$$\frac{\partial}{\partial x_j}\left(\rho\varepsilon u_j\right)=\frac{\partial}{\partial x_j}\left[\left(\mu+\frac{\mu_t}{\sigma_\varepsilon}\right)\frac{\partial \varepsilon}{\partial x_j}\right]$$
$$+\rho C_1 S_\varepsilon-\rho C_2\frac{\varepsilon^2}{k+\sqrt{\nu\varepsilon}} \quad (4)$$

where

$$C_1=\max\left[0.43,\frac{\eta}{\eta+5}\right],\quad \eta=S\frac{k}{\varepsilon},$$
$$S=\sqrt{2S_{ij}S_{ij}},\quad \mu_t=\rho C_\mu\frac{k^2}{\varepsilon},$$
$$C_\mu=\frac{1}{A_0+A_s\frac{kU^*}{\varepsilon}}$$

The model constants are $C_1=1.44$, $C_2=1.9$, $\sigma_k=1.0$, $\sigma_\varepsilon=1.2$. In these equations, σ_k and σ_ε are the turbulent Prandtl numbers for k and ε, respectively.

The velocity magnitude normal to boundary is specified at the inlet section and pressure magnitude normal to boundary is specified at outlet section, and they were used as boundary conditions to this problem and the turbulence intensity is calculated as:

$$I=0.16\left(\mathrm{Re}_{DH}\right)^{-1/8} \quad (5)$$

where Re_{DH} is the Reynolds number for pipe hydraulic diameter.

Second order discretization scheme is used for pressure, momentum, turbulence kinetic energy and turbulence dissipation rate scalar equations. The SIMPLEC (SIMPLE-Consistent) algorithm is used for the velocity-pressure coupling which is necessary to maintain the continuity throughout the iterations. Gambit fluent software is used to draw the geometry and generate the meshes as in Fig. (2).

3. Flow Rate Equations and Discharge Coefficient

The flow rate equations for orifice meter and for all differential producers (e.g. nozzle, Venturi tube) are identical. They are developed from theoretical assumptions, modified by correction factors based on empirical evidence, and further altered based on geometric considerations relative to fixed geometry.

The theoretical flow rate, Q, obtained from Bernoulli's and continuity equations is:

$$Q = \frac{1}{\sqrt{1-\beta^4}} \frac{\pi}{4} d^2 \sqrt{\frac{2\Delta p}{\rho}} \qquad (6)$$

For orifice meter, the flow rate expression obtained from Eq. (6) is not accurate expression in the actual case, and the true flow rate is almost always less than the theoretical calculated value and some correction factor, named as discharge coefficient (C_d) and expansibility [expansion] factor (e) have to be applied and the volume flow rate for orifice meter can be determined as:

$$Q = \frac{C_d}{\sqrt{1-\beta^4}} e \frac{\pi}{4} d^2 \sqrt{\frac{2\Delta p}{\rho}} \qquad (7)$$

For a given primary element, the discharge coefficient is derived from laboratory data by rationing the true and theoretical flow. The true flow rate is determined by weighing or by volumetric collection of the fluid over a measured time interval. The theoretical flow rate is calculated with Eq. (6). The discharge coefficient is then defined as:

$$C_d = \frac{True\ flow\ rate}{Theoretical\ flow\ rate} \qquad (8)$$

4. Experimental Setup

Figure 3 describes the schematic diagram of experimental setup of the flow system used in measuring the discharge coefficient of orifice plate with inner diameter (d) of 38.1 mm and a pipe diameter (D) of 63.5 mm.

A comparison method was used to compare the master flow rate measured by a traceable turbine meter, 150 to 1500 lpm, with calibration accuracy of ±0.05% of reading, traceable to National Institute of Standards and Technology (NIST) with the flow rate through the orifice meter that generates differential pressure measured by a mercury U-tube manometer with accuracy of ±0.5 mmHg at D upstream and $D/2$ downstream of orifice plate, Fig. (1). The turbine meter is installed with at least 22D upstream straight length. The theoretical flow rate was calculated by substituting the measured differential pressure, Δp, in Eq. (6) then the discharge

coefficient was calculated. A pump with discharge flow rate of 1500 lpm was used to pump water through the closed loop test rig. To control the flow rates, a throttle valve downstream of the test section was installed to control the flow rate, with a bypass pipe line installed, Fig. (3).

Flow fittings (e.g. elbow, reducer) were installed upstream of orifice meter with variable upstream length to study its effect on orifice meter readings.

5. Results and Discussion

The results are tackled and clarified into two sections: the flow structure and the effect of different fittings on the discharge coefficient.

5.1 Flow Structure

CFD gives a complete flow field structure for all fittings (e.g., reducer, single elbow, double-elbow in-plane, double-elbow out-of-plane, T-junction) with orifice plate as follows:

5.1.1 Reducer

Figure (4) shows the contours of velocity for reducer with orifice and the trend of velocity that increases after the reducer. Reducer keeps the velocity to be axisymmetric. The reducer works as subsonic nozzle resulting in pressure decrease, therefore, the average velocity increases according to the continuity equation. In this figure and upcoming figures, the x-z plane represents the horizontal plane while the x-y plane represents the vertical plane.

Figure (5) shows the difference between the computed velocity profiles for reducer installed at distances of L = 2D, 4D, 6D, 10D and 15D upstream of the orifice plate and an orifice plate with upstream straight length. All profiles are presented at section A of 1D upstream of the orifice plate at the location of the upstream pressure tap. It's appeared that the velocity profiles for L = 10D and 15D reducer installation cases have a good agreement with the velocity profile for orifice plate with straight length installation case. So, the effect of reducer decreases if it was installed at distance greater than L = 10D upstream of the orifice plate.

5.1.2 Single Elbow

For 90^{o} elbow with radius ratio equal to two, Fig. (6) shows the contours of isovelocity lines for the elbow. As the flow enters the elbow, the pressure starts to increase at the concave surface taking into account the Bernoulli's equation (energy).

This will increase the velocity at the convex surface and this effect will continue to the end of elbow where the velocity reaches its maximum at the elbow inside wall vicinity. Due to the centrifugal force, the high speed core of the flow is pushed towards the outside wall of elbow up to distance L = 5D downstream of the elbow end and L = 1D upstream of the orifice plate where the flow starts to nearly retain the normal turbulent profile and this is visible at computed velocity profile for L = 6D upstream installation case, see Fig. (7).

Figure (7) shows that computed velocity profiles for single elbow installed at L = 2D and 4D upstream of the orifice plate were greatly distorted from the normal profile (orifice only). But for L = 10D, 15D and 40D upstream installation cases, the velocity profiles are nearly identical especially for L = 15D and 40D cases but still not fully matched with that for orifice preceded by straight pipe.

5.1.3 Double-Elbow in-Plane, $L_e = 4D$

At this case, the existence of another elbow installed in opposite direction of the upstream elbow and in the same plane makes balance to the high speed core (see section 5.1.2) to be in the center of the pipe; see Fig. (8); and retain the normal profile rapidly. At this case and upcoming elbow configuration the radius ratio of all elbows equal to two.

For L = 2D and 4D upstream installation cases, Fig. (9), the computed velocity profiles are distorted and they are out of the normal profile. But for L = 6D, 10D and 15D installation cases, the velocity profiles are identical with each other and with the normal profile (orifice only) especially for L = 10D and 15D installation cases.

5.1.4 Double-Elbow in-Plane, $L_e = 0$

This installation case has the same trend of the previous case but at this case when the distance between the two elbows $L_e = 0$, is accelerated the flow to retain the normal velocity profile, Figs. (10) and (11). Even for L = 2D and 4D installation cases the velocity profile is much close to the normal profile if it is compared with the previous case.

5.1.5 Double-Elbow out-of-Plane, $L_e = 4D$

For this configuration of elbows, the contours of isovelocity lines at Fig. (12) show skew to the outer wall as in other elbow configuration. But at this configuration, Fig. (13) shows that the velocity profiles skewed to the outer wall

for installation cases up to L = 6D. Only for L = 15D installation case, the velocity profile retain the normal velocity profile but not coincident with the profile of orifice with straight length (orifice only) installation case.

5.1.6 Double-Elbow out-of-Plane, $L_e = 0$

This configuration has the same trend as the previous one in section 5.1.5 but the velocity profile for L = 2D installation case has a bad distortion from the normal velocity profile, Figs. (14) and (15). From Fig. (15) the velocity profiles for L = 10D and 15D installation cases are coincident and retains the normal velocity profile but not coincident with orifice only velocity profile.

5.1.7 T-junction

This configuration can be treated as a summation of two single shape edged elbows installed in one line, Figs. (16) and (17). The normal velocity profile was retained at L = 15D installation case as shown in Fig. (17). Also, the velocity profile for L = 15D installation case is very close to the normal velocity profile of orifice only case.

5.1.8 Fittings, L = 15D

For all previous fittings installed upstream of the orifice plate, Fig. (18) shows the computed velocity profiles for all fittings installed at a distance of L = 15D upstream of the orifice plate. It is evident that some velocity profiles of fittings retain the normal velocity curve and coincident with orifice only profile like reducer and the two configurations of double-elbow in-plane.

5.2 Effect on Discharge Coefficient

The pressure coefficient C_p across the orifice plate at D upstream and $D/2$ downstream the plate is a result of the CFD analysis as in Figs. (19) and (20), in these figures the $x/D = 0$ point is the position of orifice plate. Also, the differential pressure Δp is measured experimentally using a mercury U-tube manometer. The differential pressure was used to get the theoretical flow rate through the orifice plate using Eq. (6) and then the discharge coefficient was calculated as in section 3.

For the reducer, as the Reynolds number increases and the upstream distance between the reducer and the orifice plate increases the discharge coefficient decreases as in Fig. (21), in this figure and

upcoming figures the lines represent the trend of the computational data points of the same color.

For the single elbow, as the Reynolds number increases and the distance between orifice plate and elbow decreases the discharge coefficient decreases, Fig. (22).

For the double-elbow in-plane and $L_e = 4D$, Fig. (23) shows that at high Reynolds numbers, the discharge coefficient tends to be constant. Also, as the Reynolds number increases the discharge coefficient decreases.

For the double-elbow in-plane and $L_e = 0$, Fig. (24) shows that the configuration is similar to single elbow case.

For the double-elbow out-of-plane and $L_e = 4D$, Fig. (25) shows that the discharge coefficient trend is constant for low Reynolds numbers.

For the double-elbow out-of-plane and $L_e = 0$, Fig. (26) shows that the discharge coefficient has a small variation with change in Reynolds number.

For the T-junction, as the Reynolds number increases the discharge coefficient decreases, Fig. (27). It is similar to the single elbow case.

Other experimental results as shown in Figures (28) and (29) show the variation of discharge coefficient of orifice meter with variable Reynolds number for reducer and single elbow respectively installed at different upstream lengths L from the orifice plate.

6. Conclusions

For all fittings cases close to orifice plate with a diameter ratio of 0.6 in a 2.5 inches pipe, the velocity profile was distorted by these fittings and then retains the normal velocity profile at different pipe straight lengths and Fig. (18) is an example for different fittings installed at $L = 15D$ upstream of the orifice plate.

The study gives good agreement between experimental and computational analyses in discharge coefficient values.

The most significant conclusions drawn from the study are:

1. Upstream pipe straight length of at least 10 pipe diameters length is necessary to separate the orifice plate and reducer.
2. Upstream pipe straight length of more than 40 pipe diameters length is necessary to separate the orifice plate and single elbow.

3. Upstream pipe straight length of at least 15 pipe diameters length is necessary to separate the orifice plate and double-elbow in-plane.

4. Upstream pipe straight length of more than 15 pipe diameters length is necessary to separate the orifice plate and double-elbow out-of-plane.

5. Upstream pipe straight length of more than 15 pipe diameters length is necessary to separate the orifice plate and T-junction.

6. The discharge coefficient of the orifice is affected by the upstream distance between the orifice plate and the studied fittings up to 15D upstream distance of orifice plate and by Reynolds number.

Nomenclature

C_d Orifice discharge coefficient - Dimensionless

C_p Pressure coefficient $C_p = \dfrac{p - p_{ref}}{0.5\rho V_{av}^2}$ - Dimensionless

D Pipe diameter - m

d Orifice diameter - m

e Expansibility factor -Dimensionless

g Acceleration of gravity - m/s^2

I Turbulence intensity - Dimensionless

k Turbulence kinetic energy - m^2/s^2

L Distance between fitting and orifice plate - m

L_e Distance between two elbows - m

p Pressure - Pa

p_{ref} Reference pressure at the pipe outlet - Pa

Q Flow rate of the fluid through the orifice - m^3/s

r Radius of the point of interest from the center line - m

R Radius of the pipe - m

Re_D Pipe Reynolds number $Re_D = \dfrac{\rho V_{av} D}{\mu}$ - Dimensionless

V_{av} Average velocity - m/s

v_r r - velocity - m/s

v_θ θ - velocity - m/s

v_z z - velocity - m/s

r Cylindrical coordinate - m

θ Cylindrical coordinate - m

z Cylindrical coordinate - m

β Diameter ratio of the orifice diameter to the pipe diameter - Dimensionless

Δp Differential pressure across the orifice plate - Pa

ε Turbulence dissipation rate - m^2/s^3

μ Dynamic viscosity - Pa.s

μ_t Turbulent dynamic viscosity - Pa.s

ρ Density of the fluid at all points in the fluid - kg/m^3

σ_k Turbulent Prandtl number for k - Dimensionless

σ_ε Turbulent Prandtl number for ε - Dimensionless

References

Baker, R.C. *Flow Measurement Handbook*, Cambridge University Press, 2005.

"FLUENT 6.3 User's Guide", Fluent Inc., September 2006. http://www.ansys.com

Gersten, K. "Flow metering with disturbed inflow", *Acta Mechanica* 201(2008): 13–22.

ISO 5167-2-2003(E). "Measurement of fluid flow by means of pressure differential devices inserted in circular-cross section conduits running full, Part 2: Orifice plates".

Mattingly, G.E. and Yeh, T.T. "Effects of pipe elbows and tube bundles on selected types of flowmeters" *Flow Measurement and Instrumentation* 2 (1991): 4–l3.

Miller, R.W., *Flow Measurement Engineering Handbook*, 3rd edition, McGraw-Hill, London 1996.

Munson, B.R., and Young, D.F., *Fundamentals of Fluid Mechanics*, John Wiley & Sons, Inc., 2002.

Prabu, S.V., Mascomani, R., Balakrishnan, K., and Konnur, M.S. "Effects of upstream pipe fittings on the performance of orifice and conical flowmeters", *Flow Measurement and Instrumentation* 7(1996): 49–54.

Reader-Harris, M.J., Sattary, J.A., and Spearman, E.P. "The orifice plate discharge coefficient equation – further work", *Flow Measurement and Instrumentation* 6(1995): 101–114.

Rhinehart, R.R., Gebreyohannes, S., Manimegalai-Sridhar, U., Patrachari, A. and Rahaman, Md.S. "A power law approach to orifice flow rate calibration", ISA Transactions: *The Journal of Automation* 50(2011): 329–341.

U.S. Department of Commerce "GRI/NIST Orifice Meter Discharge Coefficient Database", National Institute of Standards and Technology, May 1994.

Yoon, J.Y., Sung, N.W., and Lee, C.H. "Effect of distance between 90° elbow close to upstream of orifice plate and the orifice plate on discharge coefficient", IMechE Part E: *Journal of Process Mechanical Engineering* 223(2009): 97–100.

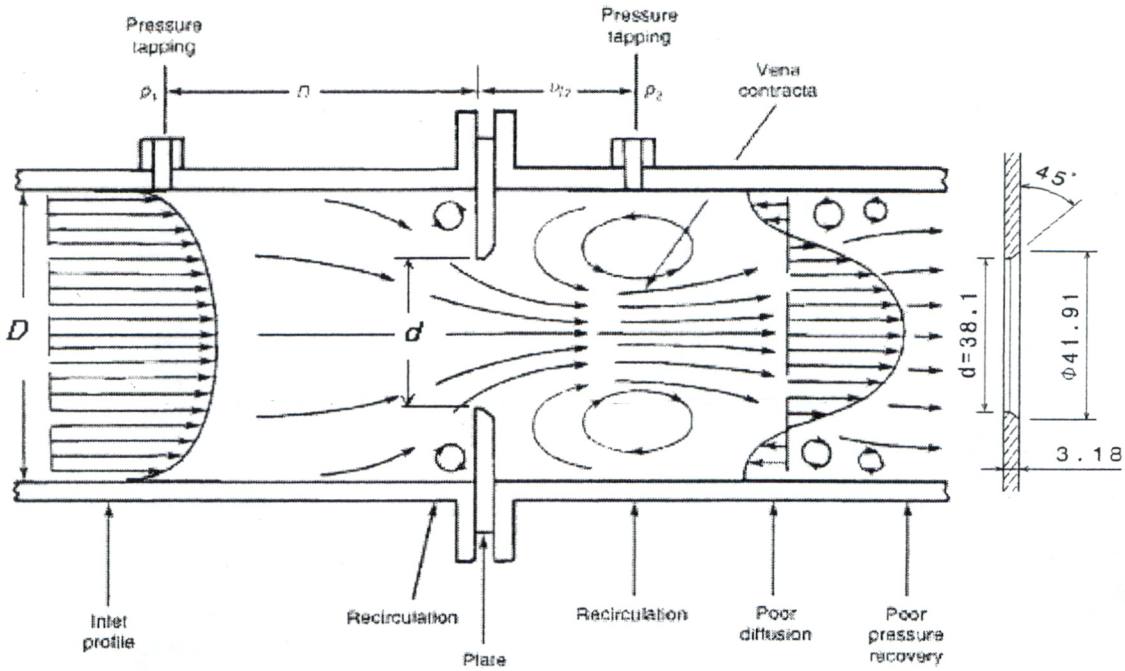

Fig. (1) Geometry and flow patterns in the orifice plate flowmeter, Baker (2005)

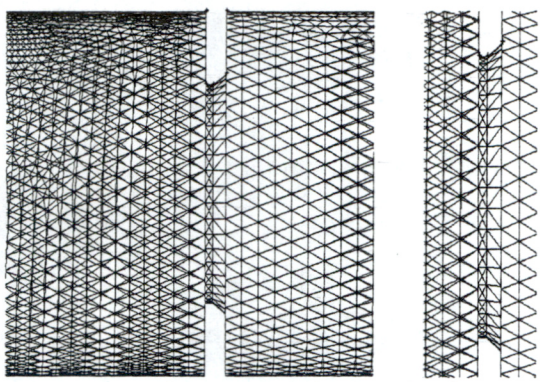

(a) Orifice

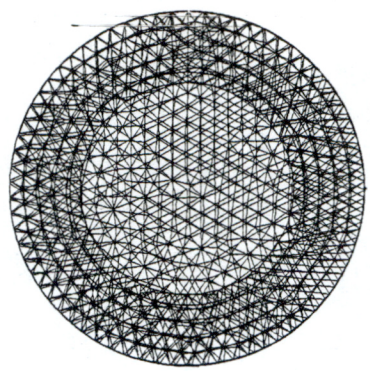

(b) Cross-section of the pipe

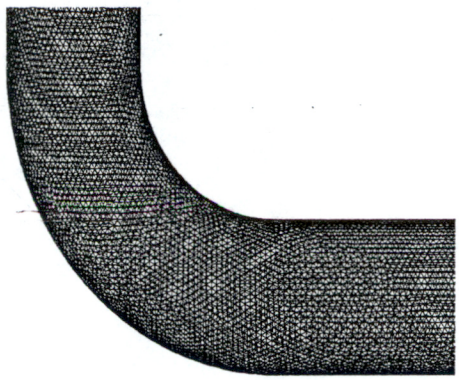

(c) Elbow

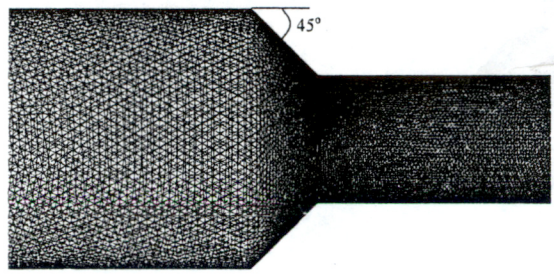

(d) Reducer

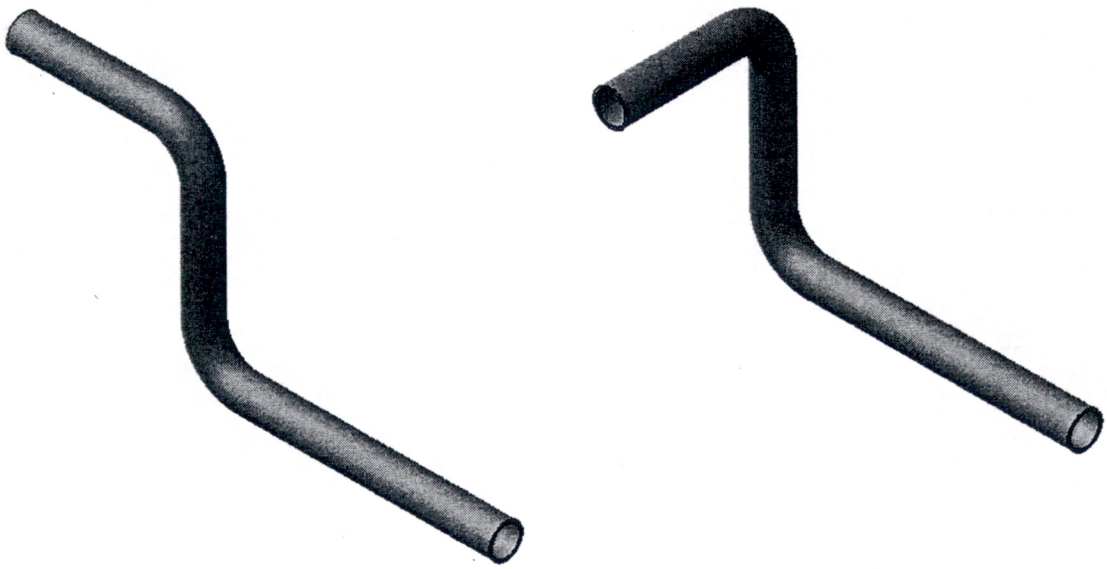

(e) Double-elbow in-plane **(f) Double-elbow out-of-plane**

Fig. (2) Meshes of orifice, pipe, elbow, reducer and other configurations of elbow

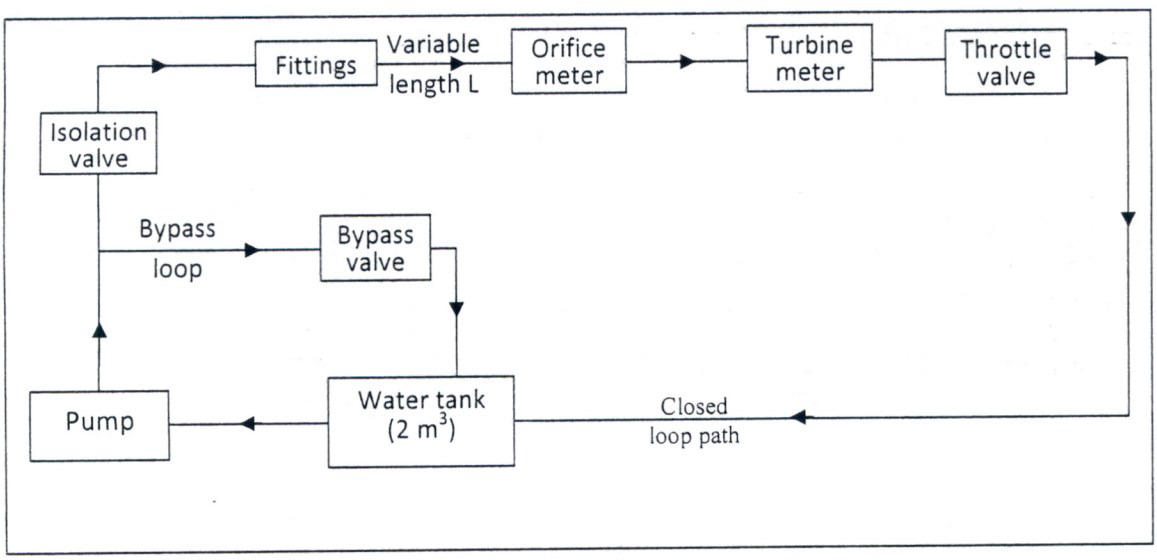

Fig. (3) Schematic diagram of flow rate test system

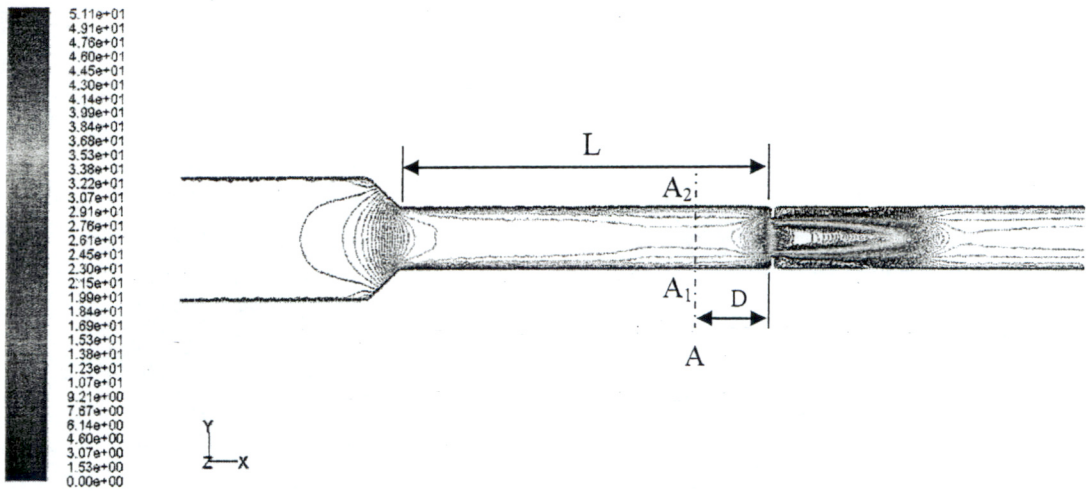

Fig. (4) Contours of isovelocity lines for reducer installed at a distance of L = 6D upstream of orifice plate

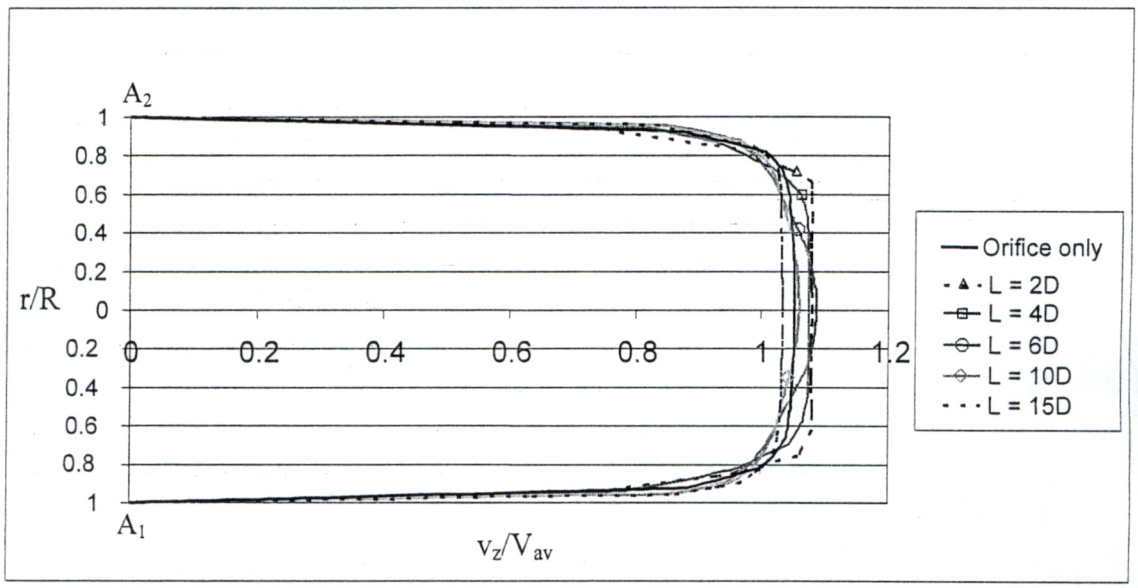

Fig. (5) Computed velocity profiles for orifice with reducer at different installation step distances L at section A

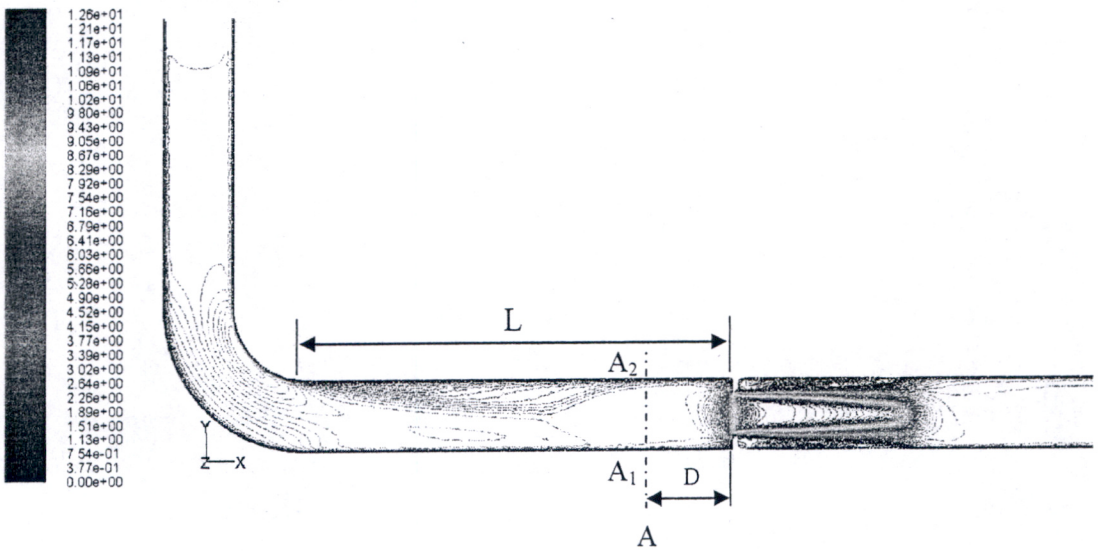

Fig. (6) Contours of isovelocity lines for elbow installed at a distance of L = 6D upstream of orifice plate

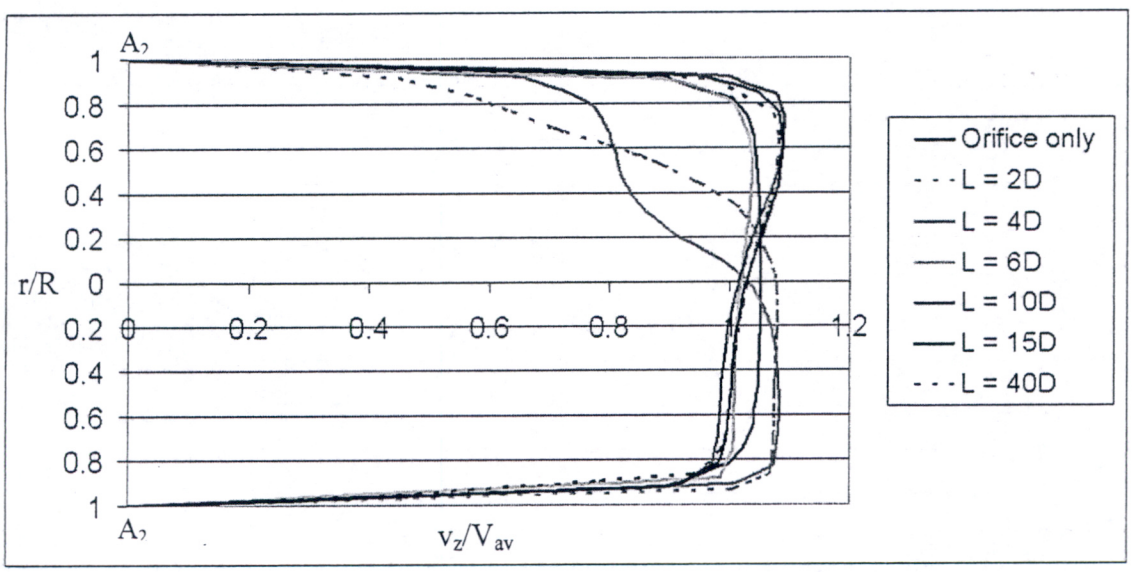

Fig. (7) Computed velocity profiles for orifice with single elbow at different installation step distances between them at section A

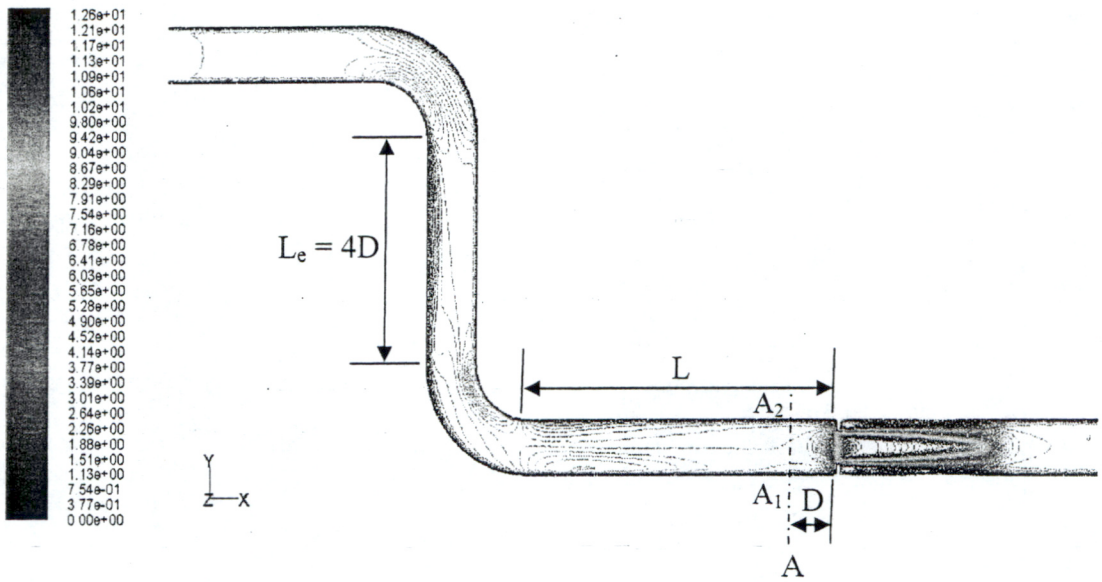

Fig. (8) Contours of isovelocity lines for double-elbow in-plane - Distance between two elbows L_e = 4D - installed at a distance of L = 6D upstream of orifice plate

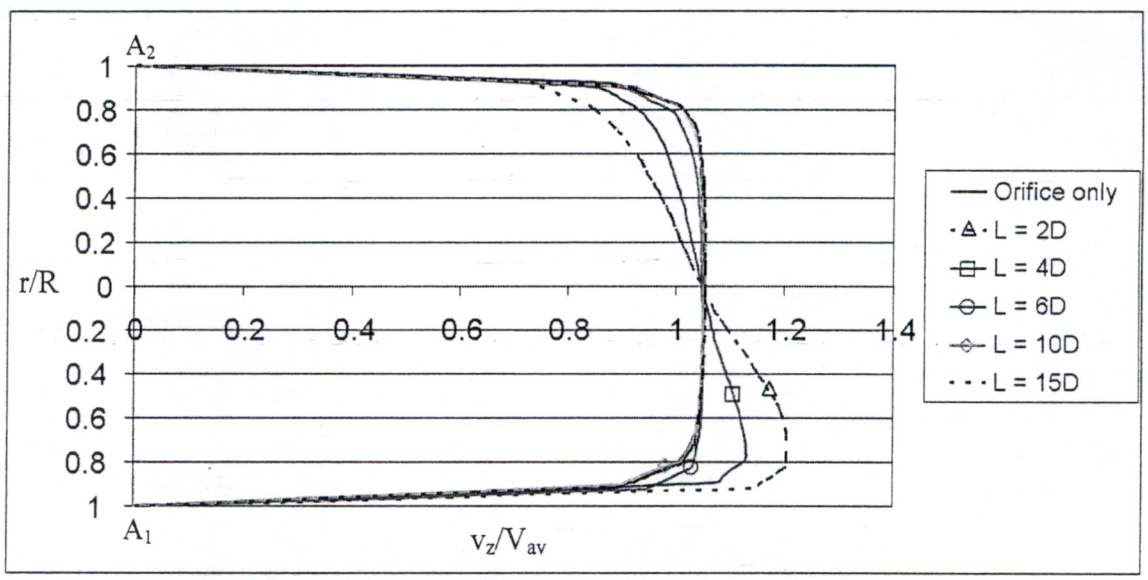

Fig. (9) Computed velocity profiles for orifice with double-elbow in-plane - Distance between two elbows L_e = 4D - at different installation step distances L at section A

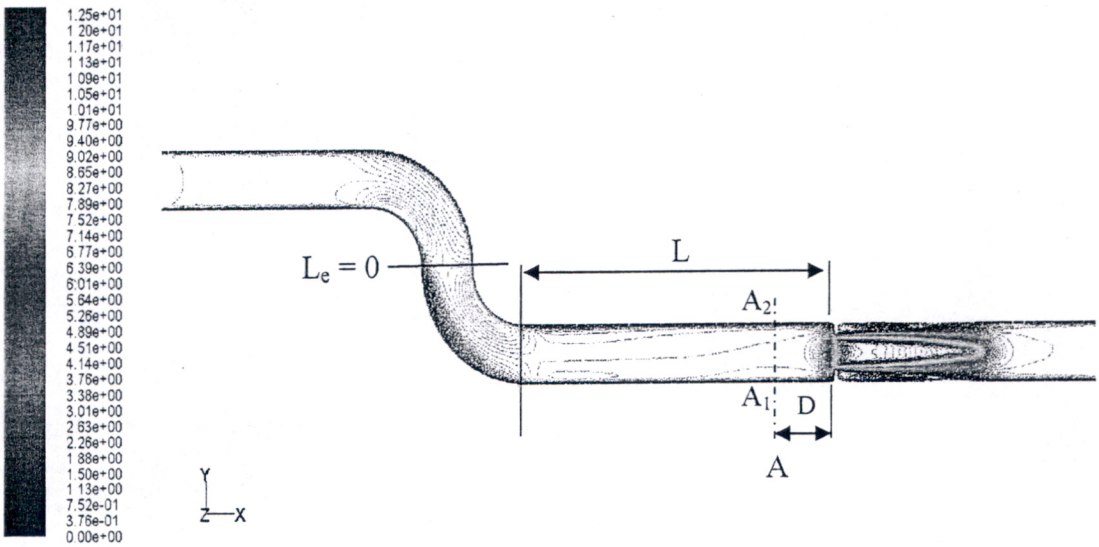

Fig. (10) Contours of isovelocity lines for double-elbow in-plane - Distance between two elbows L_e = 0D - installed at a distance of L = 6D upstream of orifice plate

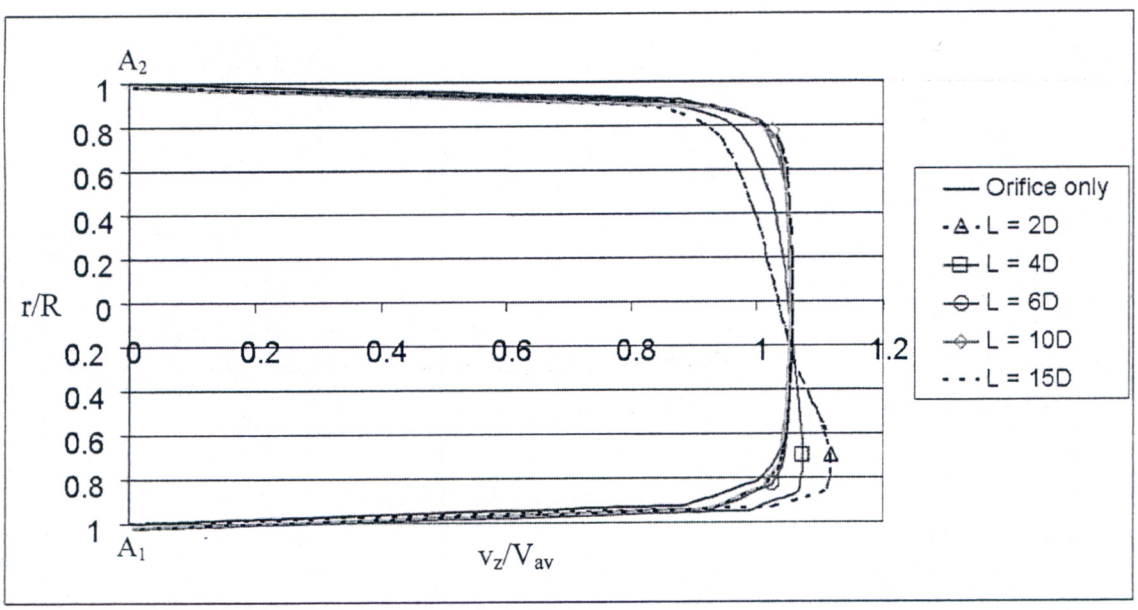

Fig. (11) Computed velocity profiles for orifice with double-elbow in-plane - Distance between two elbows L_e = 0 - at different installation step distances L at section A

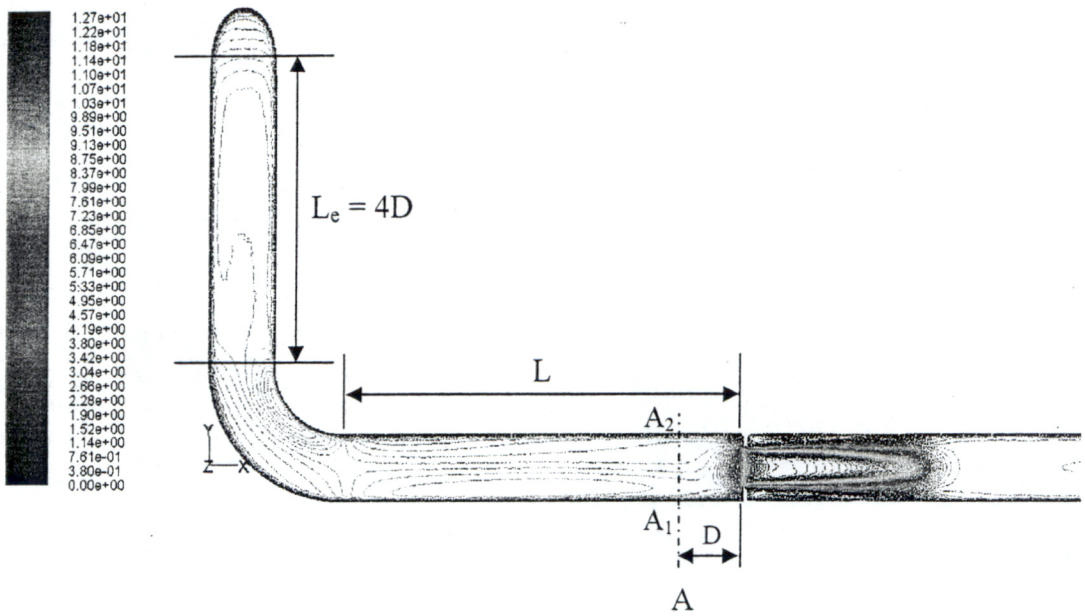

Fig. (12) Contours of isovelocity lines for double-elbow out-of-plane - Distance between two elbows L_e = 4D - installed at a distance of L = 6D upstream of orifice plate

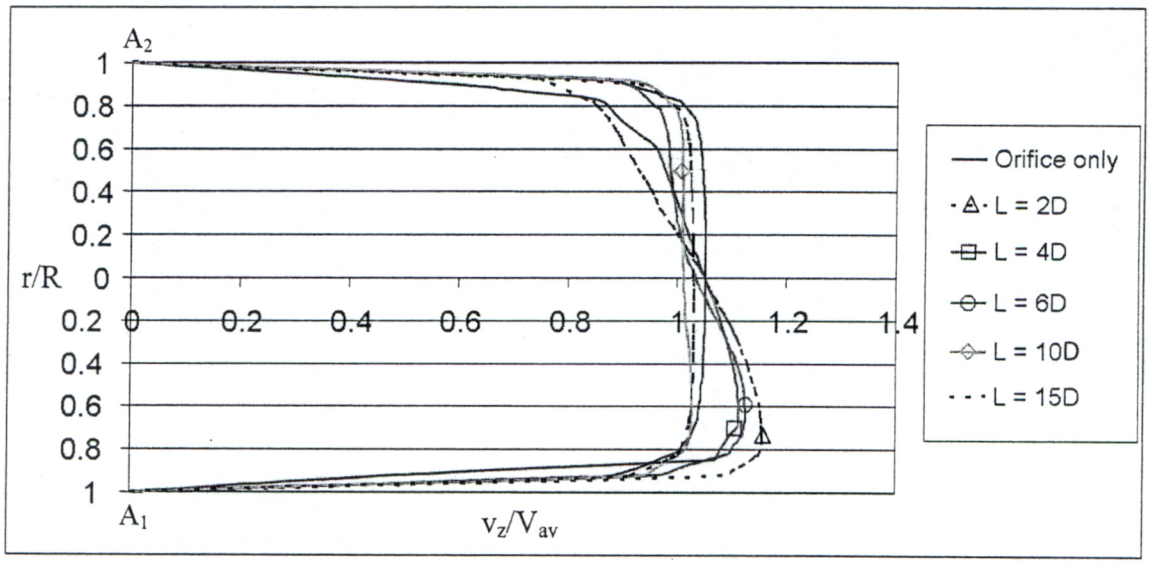

Fig. (13) Computed velocity profiles for orifice with double-elbow out-of-plane - Distance between two elbows L_e = 4D - at different installation step distances L at section A

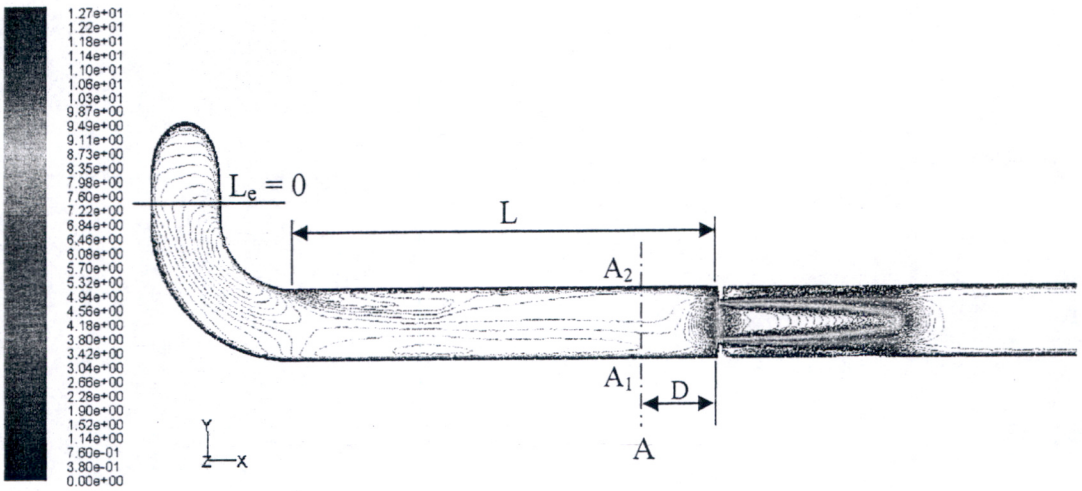

Fig. (14) Contours of isovelocity lines for double-elbow out-of-plane - Distance between two elbows L_e = 0D - installed at a distance of L = 6D upstream of orifice plate

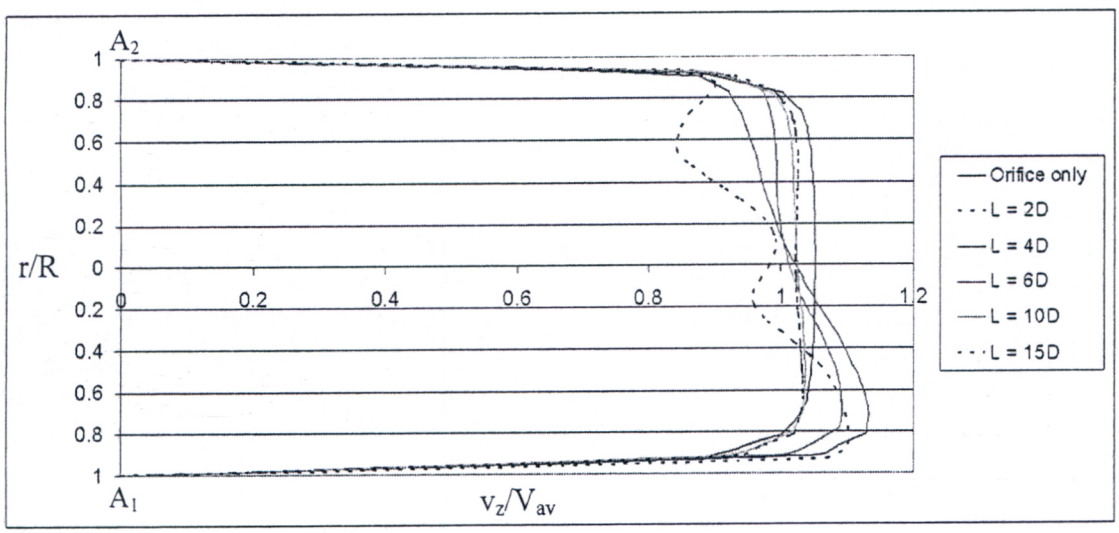

Fig. (15) Computed velocity profiles for orifice with double-elbow out-of-plane - Distance between two elbows L_e= 0 - at different installation step distances L at section A

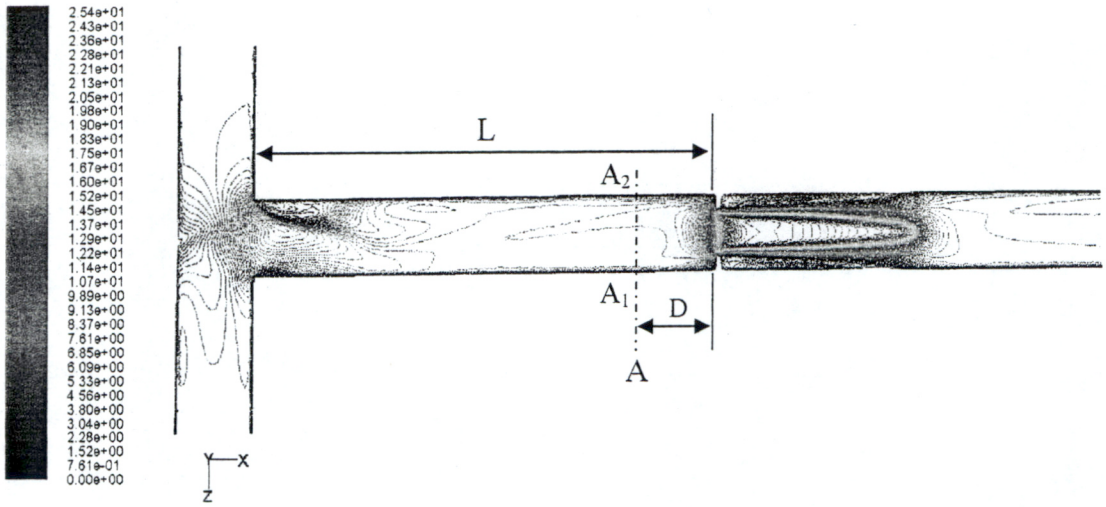

Fig. (16) Contours of isovelocity lines for T-junction installed at a distance of L = 6D upstream of orifice plate

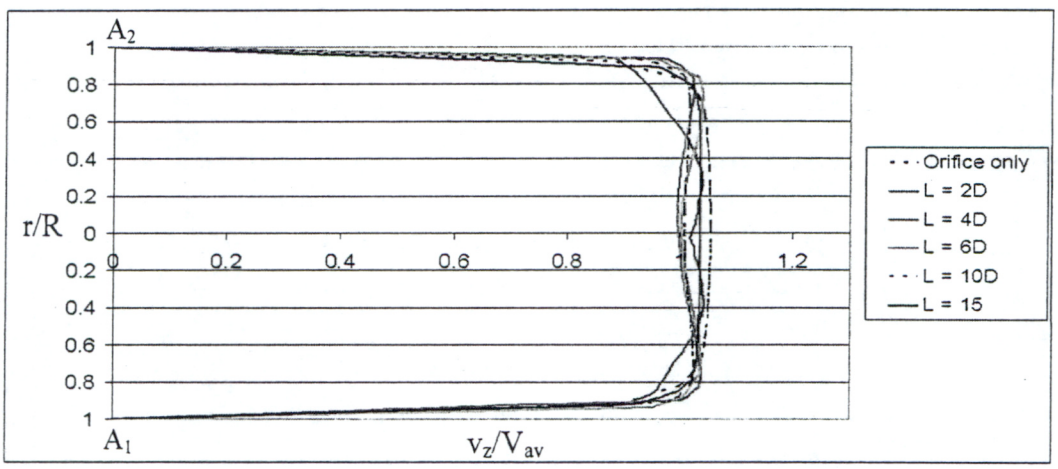

Fig. (17) Computed velocity profiles for orifice with T-junction at different installation step distances L at section A

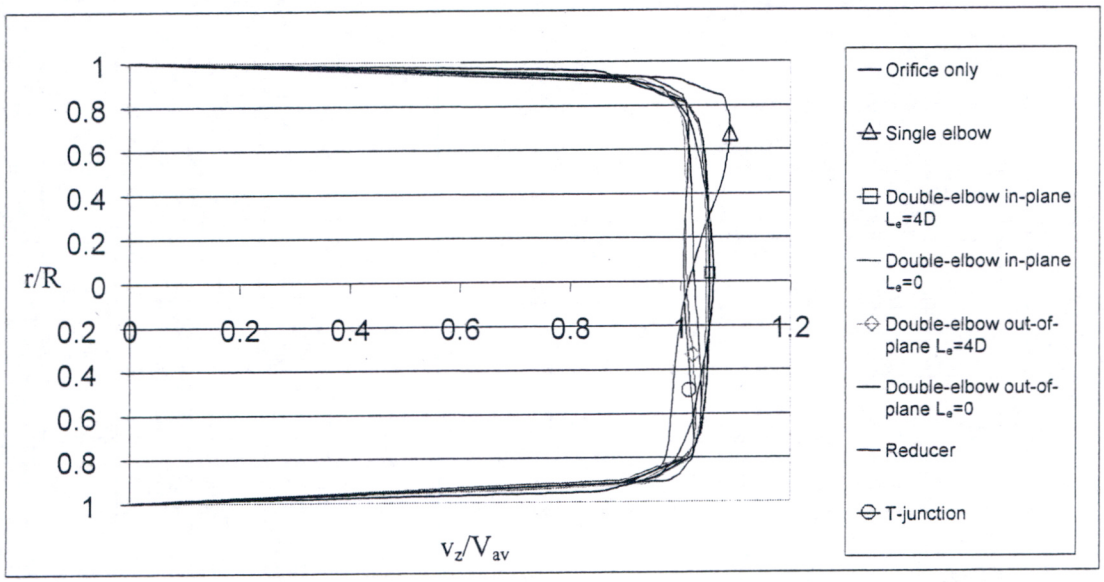

Fig. (18) Computed velocity profiles for fittings installed at L = 15D upstream of the orifice plate plotted at section A

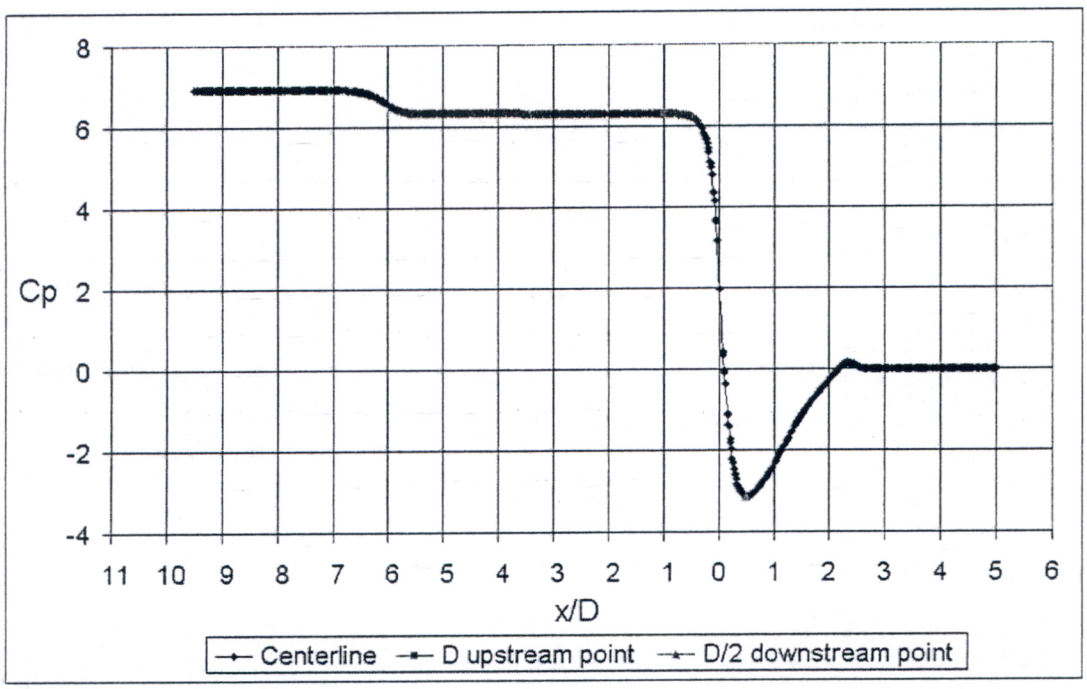

Fig. (19) Pressure coefficient along centerline of orifice with reducer installed at L = 6D. (Fluent 6.3)

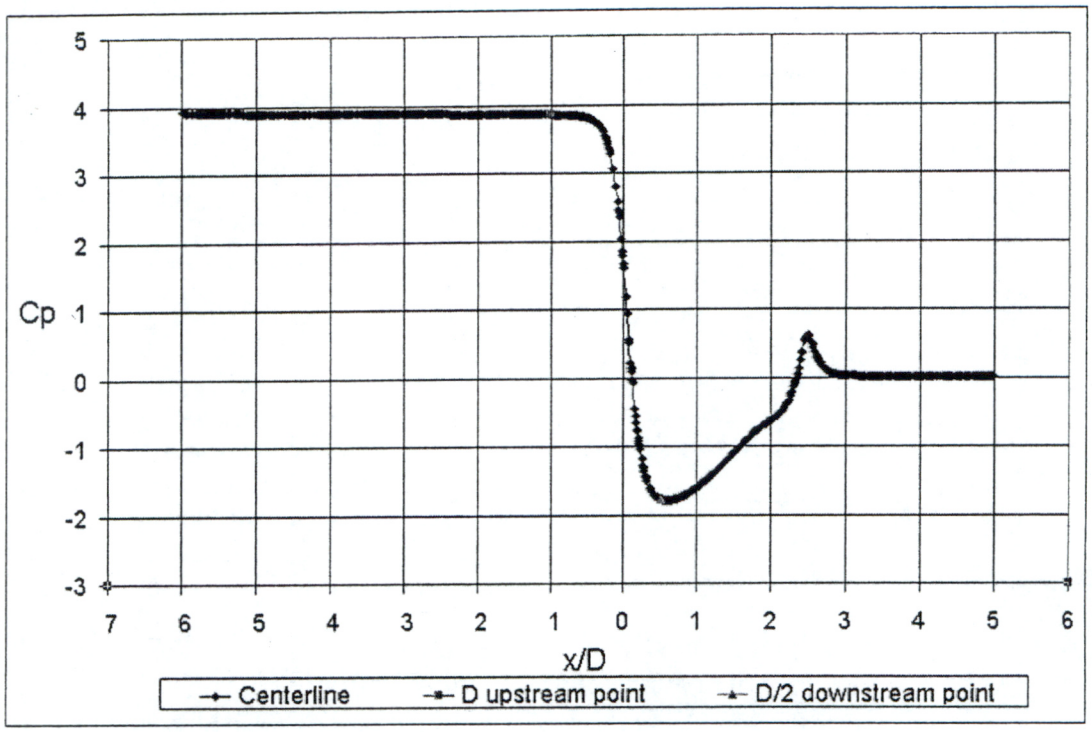

Fig. (20) Pressure coefficient along centerline of orifice with single elbow installed at L = 6D. (Fluent 6.3)

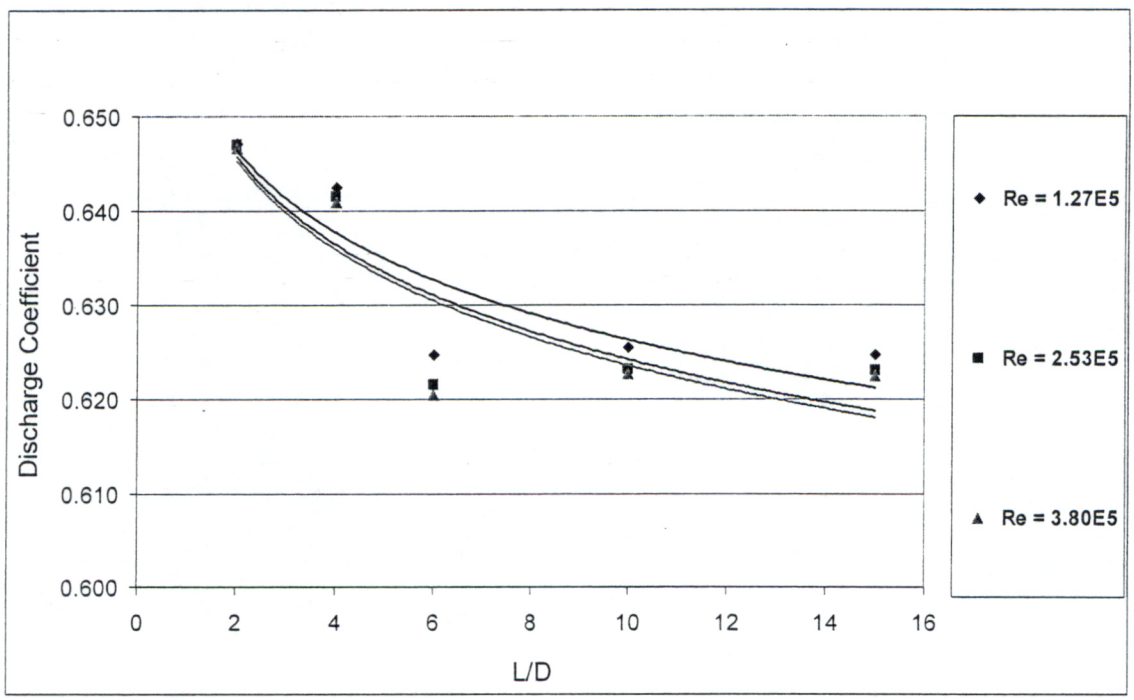

Fig. (21) Effect of reducer with variable upstream length L on orifice plate discharge coefficient corresponding to different Reynolds numbers

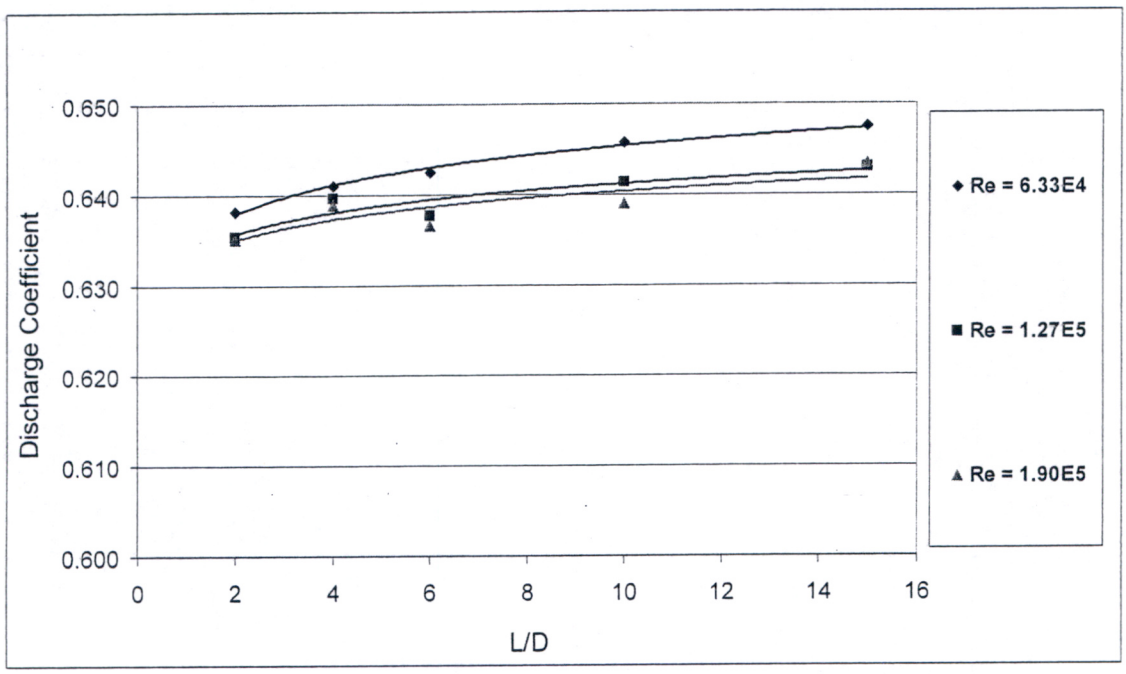

Fig. (22) Effect of single elbow with variable upstream length L on orifice plate discharge coefficient corresponding to different Reynolds numbers

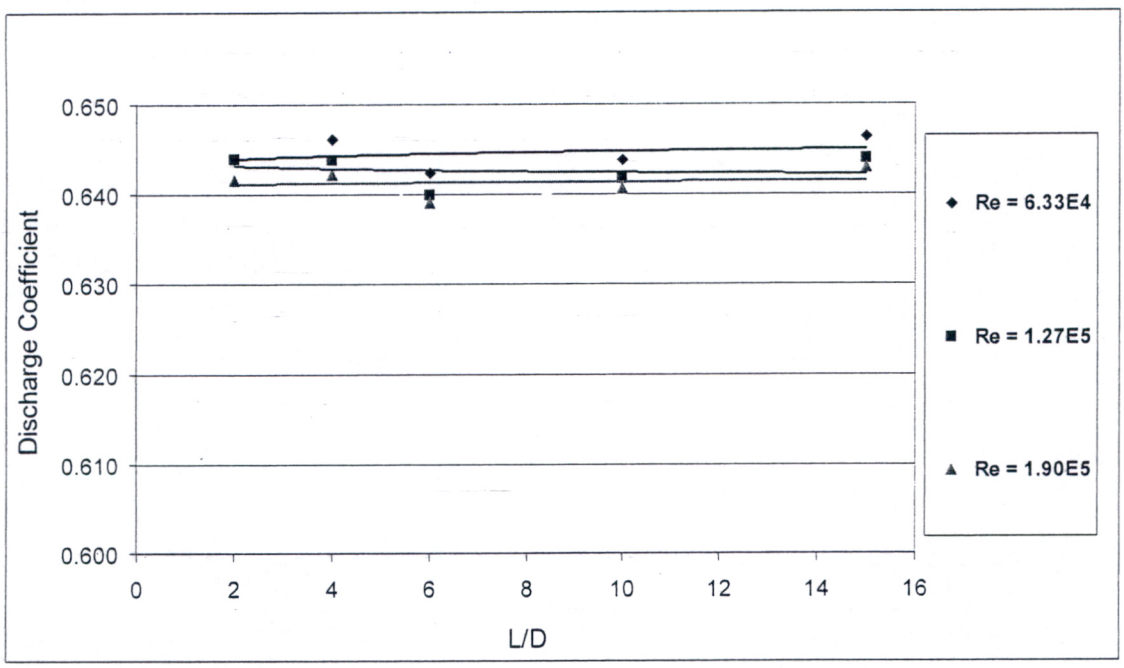

Fig. (23) Effect of double-elbow in-plane - L_e = 4D - with variable upstream length L on orifice plate discharge coefficient corresponding to different Reynolds numbers

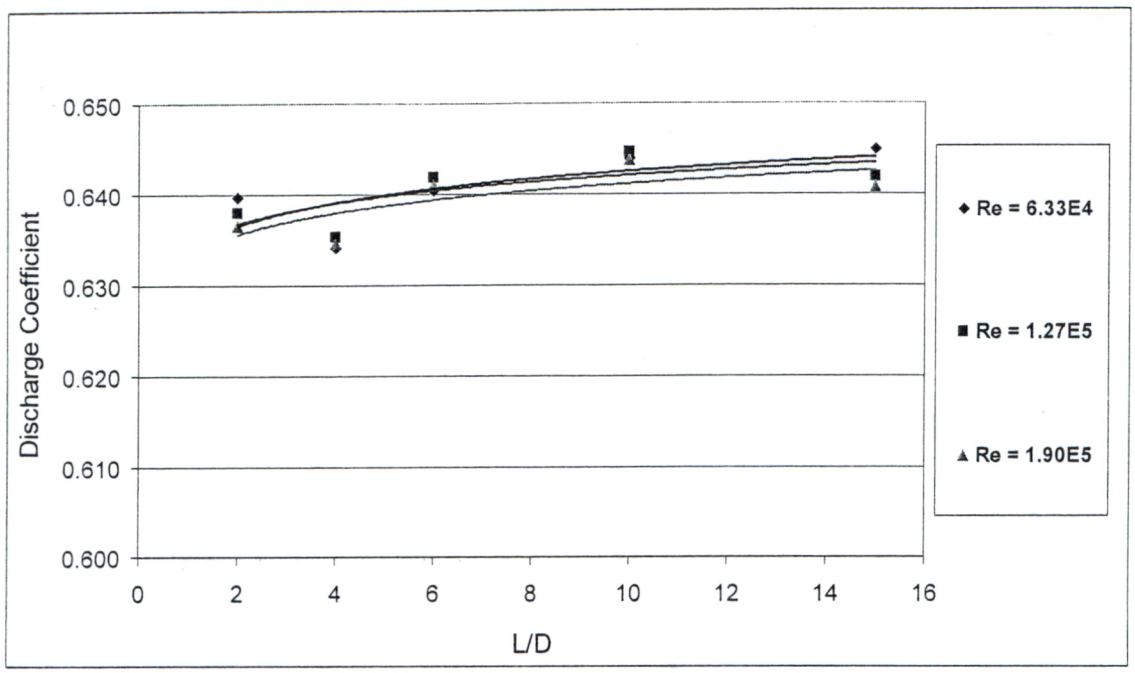

Fig. (24) Effect of double-elbow in-plane - L_e = 0D - with variable upstream length L on orifice plate discharge coefficient corresponding to different Reynolds numbers

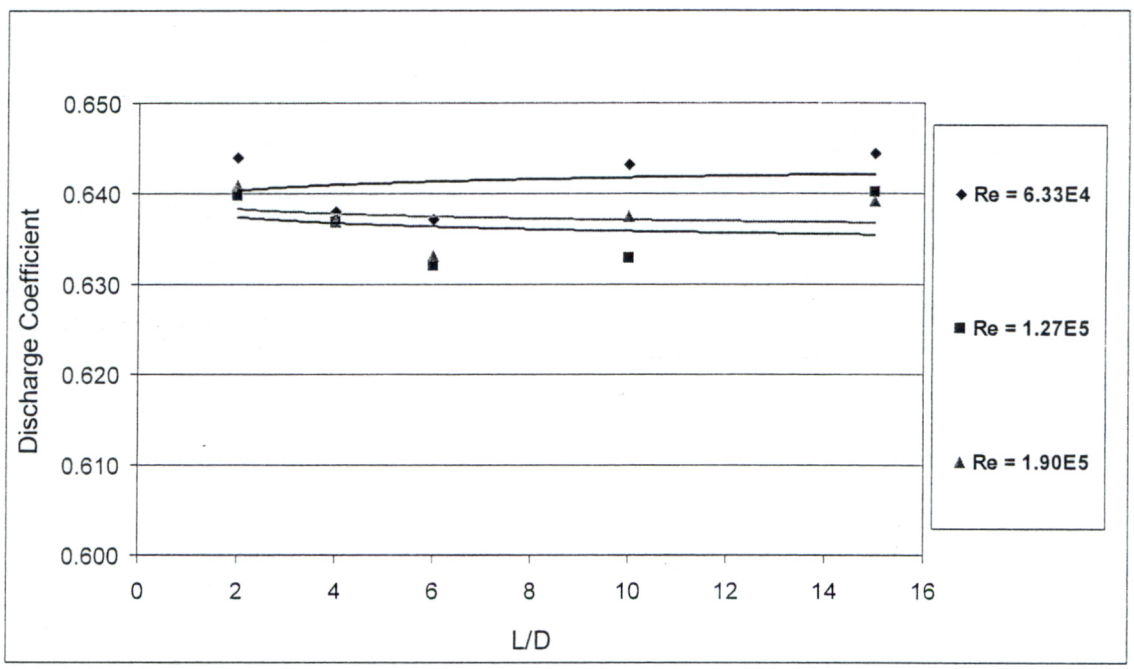

Fig. (25) Effect of double-elbow out-of-plane - L_e = 4D - with variable upstream length L on orifice plate discharge coefficient corresponding to different Reynolds numbers

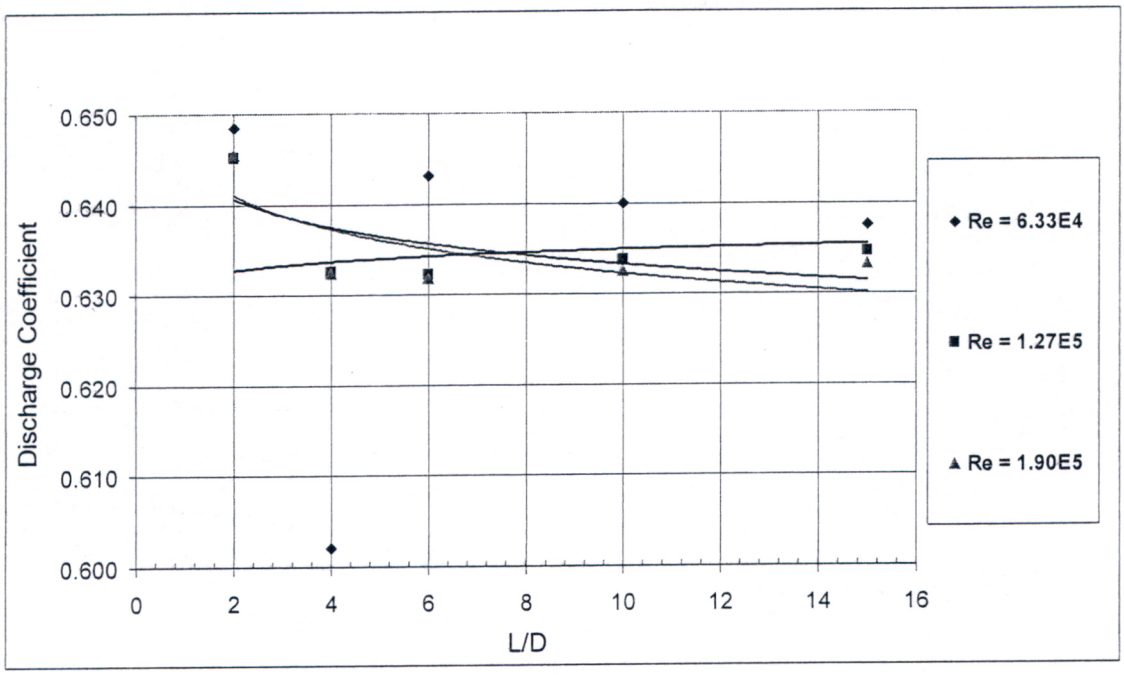

Fig. (26) Effect of double-elbow out-of-plane - L_e = 0D - with variable upstream length L on orifice plate discharge coefficient corresponding to different Reynolds numbers

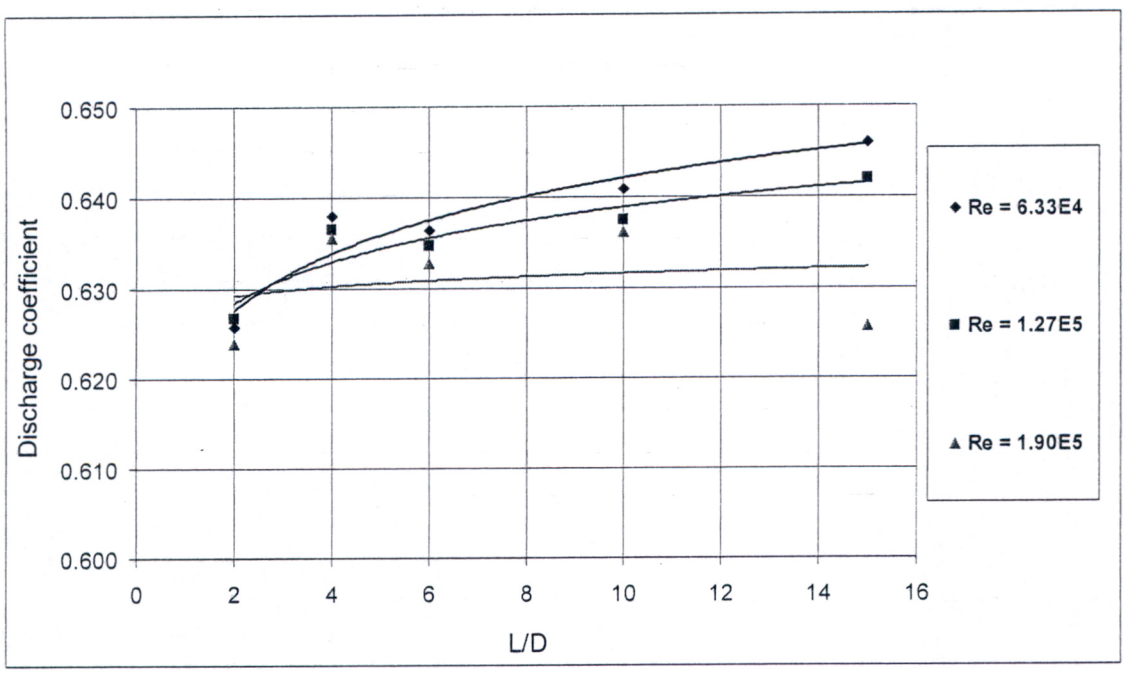

Fig. (27) Effect of T-junction with variable upstream length L on orifice plate discharge coefficient corresponding to different Reynolds numbers

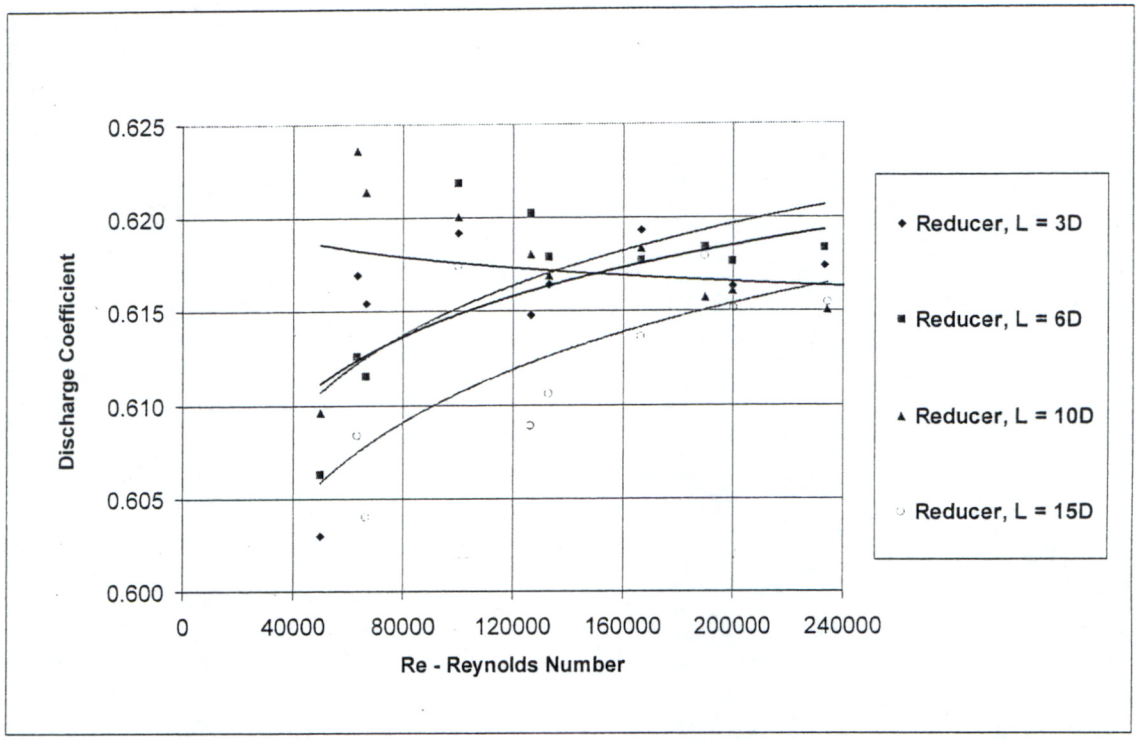

Fig. (28) Experimental data for the effect of reducer fitting with variable upstream length L on discharge coefficient

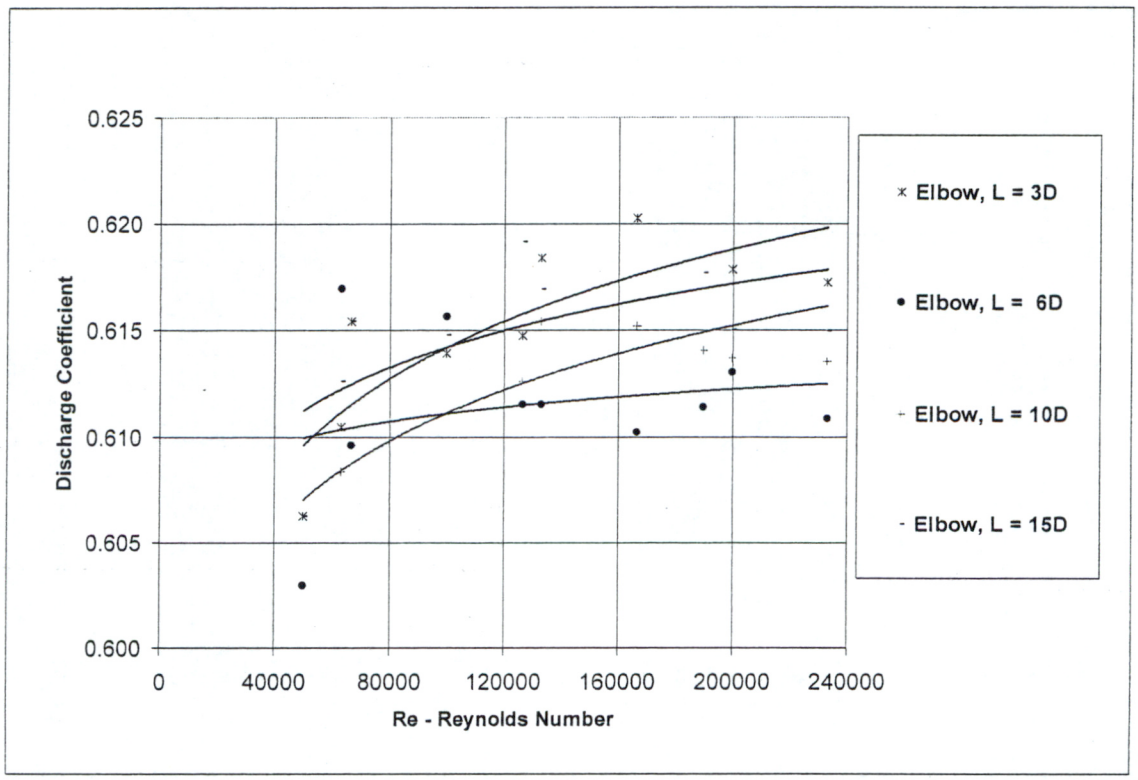

Fig. (29) Experimental data for the effect of single elbow fitting with variable upstream length L on discharge coefficient